ACS APPLIED ENERGY MATERIALS

www.acsaem.org Article

Effect of Temperature on Oxygen Reduction Reaction Kinetics for Pd Core−Pt Shell Catalyst with Different Core Size

Chen Liu, Tomoki Uchiyama,* Kentaro Yamamoto, Toshiki Watanabe, Xiao Gao, Hideto Imai, Masashi Matsumoto, Seiho Sugawara, Kazuhiko Shinohara, Koichiro Oshima, Shigeki Sakurai, and Yoshiharu Uchimoto

Cite This: https://dx.doi.org/10.1021/acsaem.0c02708 Read Online

ACCESS | Metrics & More | Article Recommendations | Supporting Information

ABSTRACT: The oxygen reduction reaction (ORR) activity and the coverage of oxide species over a Pd core−Pt shell catalyst on carbon support (Pt/Pd/C) with various Pd core sizes (2.3, 4.3, and 8.0 nm) were investigated in the temperature range from 25 to 60 °C and compared with a Pt/C catalyst (TEC10V30E, Tanaka Kikinzoku Kogyo). The apparent rate constant (k_{app}) of Pt/Pd/C increased with increasing core size at 25 °C. However, k_{app} of Pt/Pd/C started to decrease at 50−60 °C, while that of Pt/C behaved according to the general Arrhenius equation. Eventually, the 2.3 nm core showed the highest k_{app} at 60 °C, and the 8.0 nm core was almost the same as that of Pt/C. According to the electrochemical measurements, the coverage of oxide species on Pt/Pd/C was quite smaller than that of Pt/C. However, it increased dramatically with increasing temperature from 25 to 60 °C. Among the Pt/Pd/C, the 8.0 nm core showed the most obvious oxide coverage increase at 60 °C, which was almost identical to that of Pt/C. In contrast, the 2.3 nm core showed the lowest oxide coverage at 60 °C, which was expected to be the cause of the largest k_{app}. *Operando* X-ray absorption spectroscopy indicated that the Pt−Pt bond length in Pt/Pd/C was shorter than that in the Pt/C at 25 °C due to compressive surface strain from the Pd core, which is the reason why Pt/Pd/C has higher activity than Pt/C. On the other hand, as Pd has a thermal expansion coefficient higher than that of Pt, Pt/Pd/C showed a Pt−Pt bond length larger than that of Pt/C at 60 °C. A longer Pt−Pt bond length extension was observed at 60 °C in the 8.0 nm core compared to that in the other catalysts.

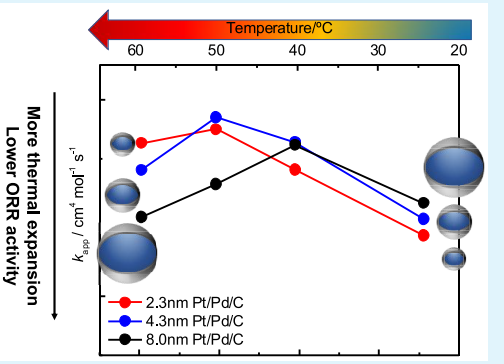

KEYWORDS: *fuel cells, core−shell catalyst, oxygen reduction reaction, operando X-ray absorption spectroscopy, temperature effect, core size effect*

Downloaded via KYOTO UNIV on January 18, 2021 at 07:53:22 (UTC).
See https://pubs.acs.org/sharingguidelines for options on how to legitimately share published articles.

INTRODUCTION

Polymer electrolyte fuel cells (PEFCs) are expected to be one of the main components of the global renewable energy system and pure hydrogen energy society of the future as they do not produce greenhouse gases during operation. Currently, PEFCs are already commercialized for low-temperature working conditions, especially in small-scale transportation systems such as fuel cell vehicles (FCVs) and residential cogeneration systems.[1−5] However, several problems remain unsolved, preventing the large-scale use of PEFCs. One major obstacle to the commercialization of FCVs is the high cost of Pt cathode catalysts used for the oxygen reduction reaction (ORR), resulting in inefficient reaction kinetics and degradation effects under the strong acidic conditions.[6−9] Therefore, high performance, high durability, and less expensive catalysts are expected to widen the use of PEFC devices.

Many studies have reported that the mass activity of Pt-based catalysts can be enhanced by increasing the active Pt surface area and changing the electronic state of Pt. Adzic's group studied Pt-based electrocatalysts synthesized by galvanic displacement of a Cu monolayer on Pd which exhibited high Pt mass activities.[10−17] Pt-based core−shell catalysts possess less Pt loading, which proved successful in the preparation of low Pt load electrocatalysts.[18−21] Core−shell catalysts also have other features that make this structure attractive, mainly because of their potential to control the ORR activity by controlling the core materials, particle size, shell thickness, and facets.[13,18,22−28] The activity of the Pt catalyst is related to the substrate-induced strain, whether tensile or compressive, in combination with the ligand effect.[29,30] The status of the *d*-band on the Pt surface layer, which is modified by ligand and strain effects, can influence the binding strength and

Received: November 1, 2020
Accepted: December 14, 2020

© XXXX American Chemical Society

absorption properties of the oxide species. Therefore, the moderate compressive strain of the Pt surface layer enhances its activity for the ORR. Among the parameters that influence the ORR activity of core−shell catalysts, core size has been demonstrated to affect activity through many ways.[13,41] The core size could affect the ORR activity by changing the active facet proportion on the Pt surface, the electronic status of shell atoms, and the lattice strain.[13,41]

Some studies have shown that the activity values evaluated for the same catalysts through MEA (membrane electrode assembly) were lower than those with RDE (rotating disk electrode) measurement, whose reasons are still under discussion.[31−37] For example, the fuel cell performances of Pd core/Pt shell catalysts (Pt/Pd/C) and the conventional Pt/C were compared through MEA measurements, and their assessment indicated that the $I-V$ performance of Pt/Pd/C was comparable to that of 50 wt %Pt/C, although the specific activity of Pt/Pd/C was higher than that of Pt/C by approximately a factor of 2 using RDE measurement in half cells with liquid electrolyte.[31] One of the differences between the RDE and the MEA measurement results may be the difference of the measurement temperature. Quantitative evaluation of ORR activities at high temperatures has been reported for pure Pt and Pt−M alloy (M = 3d transition metals) catalysts,[38,39] confirming behaviors in accordance with the general Arrhenius equation. These results indicate that temperature was not the main reason for Pt-based catalysts. In contrast, few studies have investigated the effect of temperature on Pt/Pd/C.[31] Pt/Pd/C is completely different in structure from an ordinary Pt catalyst; therefore, the different thermal behavior of the ORR activity at high temperatures may be expected to be due to the heterocontact between the Pt shell and core atoms. There is a possibility that the local structures of the Pt monolayer differ depending on the temperature and influence the status of the d-band center and the ORR activity.

Operando X-ray absorption spectroscopy (XAS) represents valuable tools to analyze the strain effects through the changes in the Pt−Pt bond length in the Pt alloy and core−shell catalysts, as reported, including our previous studies.[40−45] In general, the electrochemical properties of the catalyst have always been investigated using a thin catalyst layer on RDE. However, in most reports, *operando* XAS is conducted in the transmission mode, which requires a large amount of Pt catalyst to obtain enough signal ($\Delta\mu t \sim 1$).[41,44,46] This could cause the reaction distribution in the catalyst layer along the cross-sectional direction under the O_2-saturated electrolyte. To solve this problem, the direct measurement of XAS on the catalyst casted on RDE was performed by few researchers.[47,48]

In this study, we measured the ORR activities and the coverage of oxide species of Pt/Pd/C with different core size (2.3, 4.3, and 8.0 nm) in the temperature range of 25−60 °C. The Pt/Pd/C was synthesized by the deposition of Pt on Pd/C with galvanic displacement through underpotential deposition of Cu. *Operando* XAS was also used to observe the Pt−Pt bond distance in the catalyst and to illustrate the ORR activity temperature dependence of Pt/Pd/C. In addition, the exact same amount of catalyst loading ($\Delta\mu t \sim 0.02$) on RDE was utilized to avoid the influence of reaction distribution and ensure the correct results of *operando* XAS spectra under ORR conditions.

EXPERIMENTAL METHODS

Preparation of the Pt/Pd/C Catalyst through Cu Underpotential Deposition (Cu-UPD). Catalyst with 9.4 wt % Pd/C, 30 wt % Pd/C, and 32.2 wt % Pd/C was produced by ISHIFUKU Metal Industry Co., Ltd. Japan. The average particle size of each catalyst was 2.3, 4.3, and 8.0 nm for 9.4 wt % Pd/C, 30 wt % Pd/C, and 32.2 wt % Pd/C, respectively, as confirmed by the transmission electron microscopy image in Figure S1. The Pd/C catalyst ink consisted of a 2:3 ratio of water/2-propanal (99.99%, Wako), and the amount of Pd/C was adjusted to form a 5 μg_{Pd} cm^{-2} catalyst layer after 5 μL was dropped on a glassy carbon rotating disk electrode (GC RDE) (HOKUTO DENKO, area = 0.196 cm^2). The ink on the RDE was dried at 700 rpm at 25 °C. Subsequently, Nafion solution was dropped on the RDE surface up to a thickness of 200 nm at 25 °C. The Pt/Pd/C was prepared by depositing Pt through galvanic displacement by Pt of an underpotentially deposited (UPD) Cu monolayer. The UPD measurements were carried out in a three-electrode cell at 25 °C. The counter electrode was a Pt mesh, and the reference electrode was a reversible hydrogen electrode (RHE). After the deposition of Cu from 10 mM $CuSO_4$ in a 0.1 M $HClO_4$ solution, the RDE was rinsed with N_2-saturated water to remove Cu^{2+} from the solution and placed in a N_2-saturated 5.0 mM K_2PtCl_4 aqueous solution. After immersion for 8 min to completely replace Cu with Pt, the RDE was rinsed again with N_2-saturated water. A commercially available 30 wt % Pt/C catalyst (TEC10 V30E, Tanaka Kikinzoku Kogyo) was used as the reference sample. Figure S2 illustrates the cyclic voltammograms (CVs) for the underpotential deposition of Cu on various Pd/C in 0.1 M $HClO_4$ with 10 mM $CuSO_4$. It shows the typical CV for underpotential deposition of Cu on Pd.[49] From this result, the potential was held at 0.31 V (*vs* RHE) during underpotential deposition of Cu. Each Pt/Pd/C was denoted as Pt/Pd(d)/C, d = 2.3, 4.3, and 8.0 nm, where d indicates the average particle size of Pd in this study.

Electrochemical Measurements. As shown in Figure S3, ORR activity measurements were carried out in a three-electrode water jacket cell connected with a hot water circulator, controlling the temperatures between 25 and 60 °C. The temperature was monitored with a platinum resistance thermometer. It was hard to warm up the solution over 70 °C without the evaporation of electrolyte, which makes it almost impossible to evaluate the accurate ORR activity of the catalysts.

The counter electrode was a Pt mesh, and the reference electrode was an RHE. The RHE was prepared by immersing a Pt wire in the electrolyte in a glass tube equipped with inlet and outlet ports for H_2 gas. The RHE was inserted in the main electrochemical cell. Prior to the catalyst activity measurements, the potential was cycled 20 times between 0.02 and 1.1 V (*vs* RHE) at 100 $mV{\cdot}s^{-1}$ to obtain a stable cyclic voltammogram in N_2-saturated 0.1 M $HClO_4$. The final cyclic voltammogram was obtained at 50 $mV{\cdot}s^{-1}$. After the measurements, the electrolyte was saturated in O_2. As Pd metal may have hydrogen storage properties even in the nanoparticles, we set the cyclic voltammogram range starting from 0.1 V *vs* RHE. The different CV ranges among Pd/C, Pt/C, and Pt/Pd/C were adopted from the article from Adzic's group.[17] Data regarding oxygen reduction for all materials studied were analyzed using the Koutechy-Levich equation at 0.9 V *vs* RHE. The ORR activity was evaluated by preparing a sample for each temperature with the same method as described above and evaluated at least five times at every temperature. Cyclic voltammograms during the Cu underpotential deposition process are shown in Figure S4. In addition, the chronoamperogram of the corresponding Cu underpotential deposition process is shown in Figure S5. These results also have no significant difference among five process times, and the average Pt loading was 0.85 μg on the 0.196 cm^2 electrode area (4.3 μg_{Pt} cm^{-2}). We also measured the activity of each catalyst at each temperature 4−5 times, and the linear sweep voltammetry curves are shown in Figures S6 and S7. There was also almost no difference, indicating the high reproducibility of our experiment. The Pt loading of the Pt/C catalyst on RDE was 5 μg_{Pt} cm^{-2}.

https://dx.doi.org/10.1021/acsaem.0c02708
ACS Appl. Energy Mater. XXXX, XXX, XXX−XXX

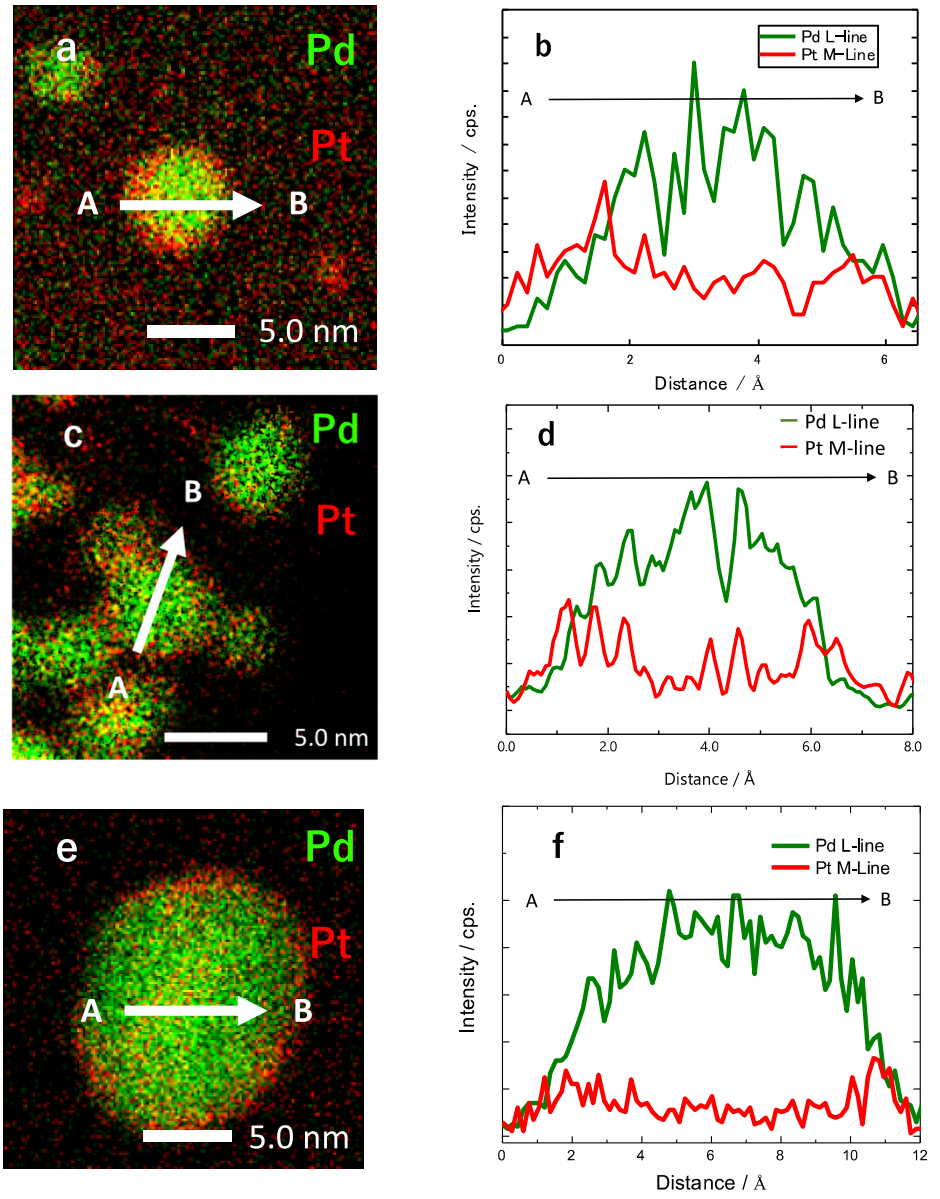

Figure 1. EDX elemental mappings and EDX line profiles of Pt/Pd/C: Pt and Pd EDX mappings of Pt/Pd(2.3)/C (a), Pt/Pd(4.3)/C (c), Pt/Pd(8.0)/C (e), showing arrow from A to B for the collection of EDX line profile data; (b,d,f) EDX line profile from A to B across the area indicated in (a,c,e).

The coverage of oxide species was measured by linear sweep voltammetry in N_2-saturated 0.1 M $HClO_4$. First, the potential was swept from 0.4 V (*vs* RHE) to the target potential (0.5−1.1 V *vs* RHE) at 50 $mV \cdot s^{-1}$, and then the potential was maintained for approximately 5 min to obtain a stable current. Finally, the potential was again set to 0.4 V (*vs* RHE). The integrated cathodic current was used to estimate the charge of oxide species based on the following reaction ($Pt{-}OH + H^+ + e^- \rightarrow Pt + H_2O$) also reported from other researchers.[50,51] The coverage of oxide species was estimated by dividing the charge of the oxide species by the underpotential deposition charge of hydrogen.[50,51] The profiles for Pt/C are shown in Figure S8 as an example.

***Operando* XAS Measurements.** *Operando* XAS measurements of the Pt L_{III}-edge of the Pt/C and Pt/Pd/C catalysts were carried out using synchrotron radiation at the beamlines BL37XU and BL01B1 at SPring-8, Hyogo, Japan. The ring current was operated at 8 GeV, with a ring current of 100 mA in the top-up mode. The measurement scheme is shown in Figure S9. Figures S10 and S11 show the details of the *operando* cell. The material for the main body of the *operando* cell is made of polyether ether ketone. The catalyst-coated RDE can be set on the center of the cell as the working electrode. The Ag/AgCl electrode (RE-8, EC Frontier CO., Ltd., Japan) and carbon rod (3 mm φ, Tokai Carbon CO., Ltd., Japan) were used as reference and counter electrodes, respectively. The polytetrafluoroethylene tube on the bottom right part is for the O_2 gas inlet to the 0.1 M $HClO_4$ electrolyte to control the gas atmosphere. The check valve (MFTD-6 V, AS ONE Corporation, Japan) is the gas outlet and also can prevent the internal pressure increase during bubbling of the gas. A 25 μm Kapton film was used as the X-ray window. The temperature was controlled by blowing heated air into a cell surrounded by a heat-insulating shield. The temperature was monitored by a platinum resistance thermometer through the check valve.

Data processing was performed using ATHENA and ARTEMIS, a suite of IFEFFIT software programs. We used the same catalyst-loaded RDE described above as a measurement sample.

Transmission Electron Microscopy. Transmission electron microscopy (TEM) and elemental mapping images were obtained using a JEM-F200 instrument and a silicon drift detector (JEOL Ltd.) at 200 kV.

https://dx.doi.org/10.1021/acsaem.0c02708
ACS Appl. Energy Mater. XXXX, XXX, XXX−XXX

X-ray Photoelectron Spectroscopy. X-ray photoelectron spectroscopy (XPS) was performed on a PHI Quantum 2000 system (ULVAC-PHI, Inc., Japan), using a monochromated Al Kα X-ray source operating at 40 W and 1486.6 eV.

High-Temperature X-ray Diffraction. A high-temperature X-ray diffraction (HT-XRD) was measured at BL02B2 and BL19B2 at SPring-8, Hyogo, Japan. The energy of the incident X-ray was 20 keV, and the samples were fixed in a quartz tube.

RESULTS AND DISCUSSION

TEM Observation and XPS Measurements. The TEM images and energy-dispersive X-ray (EDX) spectroscopy maps of Pd and Pt in Figure 1 show the observation results of as-synthesized Pt/Pd/C. The EDX maps and their line profiles confirmed the formation of a Pt shell on the Pd core, indicating the success of the Pd core/Pt shell structure, similar to another report.[22] The as-prepared Pt/Pd/C core−shell catalyst possesses an atomic ratio of Pt/Pd = 41/59, 32/68, and 29/71 for Pt/Pd(2.3)/C, Pt/Pd(4.3)/C, and Pt/Pd(8.0)/C, respectively, from the evaluation of EDX analysis.

According to XPS results in Figure S12a, the single 4f peak of Pt/Pd/C shifted to a higher binding energy (71.6 eV) compared with that of the Pt/C (71.3 eV). The peak position results are close those in another report.[52] The change of binding energy may be contributed by the coupling of electrons between the Pt shell and the Pd substrate. The compressive strain effect of the Pt shell on the Pd core could be another factor leading to the positive binding energy peak shift of Pt 4f in the Pt/Pd/C catalyst.

Electrochemical Measurements. Figure S13 shows the cyclic voltammograms for Pt/C and Pt/Pd/C at various temperatures (25−60 °C). All catalysts exhibited slight changes in hydrogen adsorption/desorption behavior depending on the temperature. This may be related to the temperature dependence of the Pt−H bond energies on different Pt crystal planes, although the details are still under investigation.[53] In addition, the oxidation of Pt was enhanced in both catalysts as the temperature increased.

The ORR activity was investigated at different reaction temperatures (25−60 °C) for Pt/C and Pt/Pd/C. The linear sweep voltammograms and the specific/mass activities were summarized in Table S2, respectively. Pt/Pd/C catalysts with various Pd core sizes exhibited the higher activity than Pt/C at 25 °C due to the compression effect from Pd core.[41] The specific and mass activity increased as the temperature increased for both catalysts. The Tafel plots of Pt/Pd/C were shown in Figure S14. The Tafel slopes of Pt/Pd/C were about 75 mV/decade higher than 0.85 V (*vs* RHE) and 143 mV/decade lower than 0.85 V, which was in agreement with other reports.[54,55] In addition, the Tafel slopes did not change among Pt/Pd/C regardless of core size and temperature, indicating that there is no significant change of the ORR mechanism. However, with increasing temperature, O_2 concentration in the solution decreases.[38] Hence, any comparison of ORR activities requires prior corrections. We introduced the correction methods and equations proposed by Wakabayashi *et al.*,[38] which allow the calculation of the apparent rate constant (k_{app}) as an indication of the reaction kinetics and activity. The summarization about the physical meaning of the parameters and the solid theoretical basis about apparent rate constant (k_{app}) and the O_2 concentration correction at different temperature are shown in the Supporting Information.

A comparison of the apparent rate constants k_{app} for the Pt/Pd/C and Pt/C at various temperatures with the Arrhenius plots is shown in Figure 2. Pt/C showed linear relationships

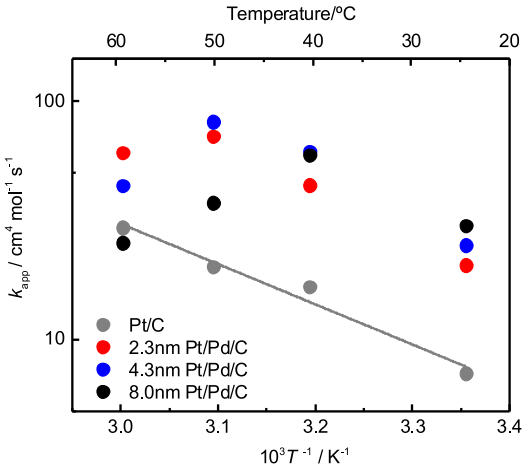

Figure 2. Arrhenius plots for the apparent rate constant k_{app} of Pt/Pd/C catalyst synthesized on 2.3 nm (red), 4.3 nm (blue), and 8.0 nm (black) diameter Pd core and Pt/C nanoparticle catalyst at 25, 40, 50, and 60 °C at 0.90 V *vs* RHE.

based on the Arrhenius equation, and the apparent activation energy was 34 kJ·mol^{-1}, which is in good agreement with previous reports.[38,39] At 25 °C, the k_{app} of the Pt/Pd/C increased with increasing Pd core size. This might be due to the moderate compression effect from the Pd core that was realized in Pt/Pd(8.0)/C. This kind of core size dependence on ORR activity was also reported.[18] Upon increasing the temperature from 25 to 60 °C, the k_{app} of each Pt/Pd/C showed different trends depending on the core size, whereas the behavior of Pt/C could be described by a simple Arrhenius equation. A clear core size dependence on the ORR activity was observed as the temperature increased. The activity of Pt/Pd(2.3)/C was the lowest compared to that of the other catalysts at 40 °C, and its plot shows a peak at 50 °C. Subsequently, the activity decreased at 60 °C, although Pt/Pd(2.3)/C had the highest k_{app} among the three catalysts. In addition, Pt/Pd(4.3)/C possessed the highest ORR activity among the catalysts at 50 °C, but it decreased at 60 °C. Moreover, Pt/Pd(8.0)/C started losing its activity at 40 °C, which was the lowest temperature among the catalysts and had the lowest ORR activity at 60 °C. These results seem to be significant because the trends of ORR activity at 25 °C were opposite to those at 60 °C when Pt/Pd/C was used. ORR activity of Pt/Pd/C was also measured upon cooling from 60 to 25 °C, indicating that there is no significant loss of ORR activity after high temperature measurement, as shown in Figure S15. Each Pt/Pd/C still possessed activity close to that of the fresh sample even after measurement at 60 °C. Therefore, the activity decay of Pt/Pd/C is not caused by degradation at 60 °C.

To investigate the loss of k_{app} at elevated temperatures in the Pt/Pd/C, the coverage of oxide species was estimated through electrochemical measurements at different temperatures and potentials. As shown in Figure 3a, the coverage of the Pt/C increased over 0.8 V (*vs* RHE) because of the formation of oxide species, which is consistent with previous reports.[50,51] The coverage exceeds 1.0 over 1.0 V (*vs* RHE) because the surface is almost fully covered with Pt−OH species and starts

https://dx.doi.org/10.1021/acsaem.0c02708
ACS Appl. Energy Mater. XXXX, XXX, XXX−XXX

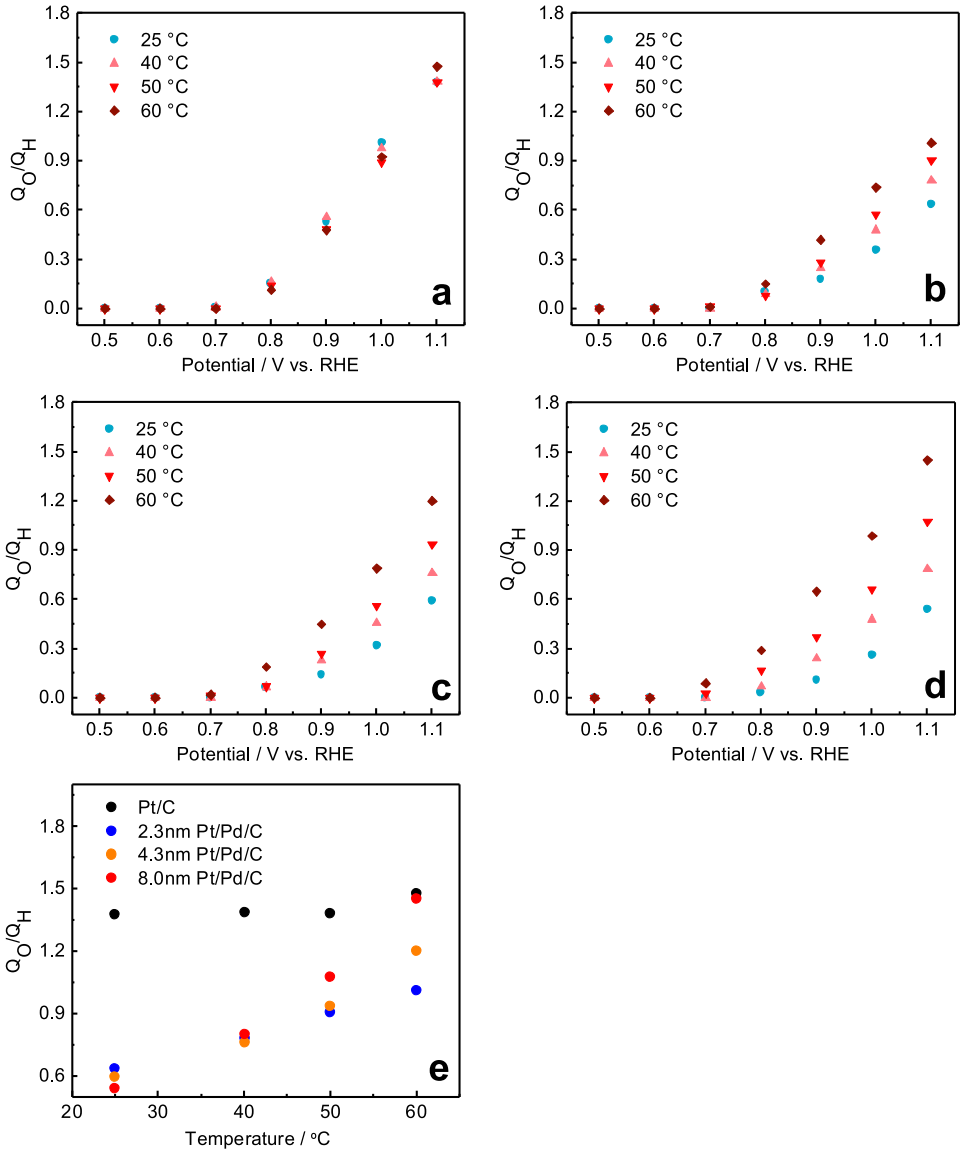

Figure 3. Oxide coverage of Pt/C catalyst (a) and Pt/Pd/C catalysts synthesized on 2.3 nm (b), 4.3 nm (c), and 8.0 nm (d) at various potentials and temperatures (0.5−1.1 V, 25−60 °C) and (e) oxide coverage of the catalysts at 1.1 V *vs* RHE.

to transform into a Pt−O species,[50,51] occupying the active sites on the Pt surface and preventing the ORR process. In the case of Pt/Pd/C in Figure 3b−d, the coverage of Pt/Pd/C was significantly smaller than that of Pt/C at 25 °C over 0.8 V. This suggested that there were less oxygen species which adsorbed on the Pt active sites in Pt/Pd/C than in Pt/C. As the oxygen species adsorbed on the Pt sites hinders ORR, the higher activity can be expected in the smaller coverage.[10−15,27,28] Therefore, a larger value of k_{app} in the Pt/Pd/C compared to that in the Pt/C was obtained at 25 °C. However, the oxide coverage of Pt/Pd/C increased dramatically for the temperatures above 40 °C. Figure 3e shows a comparison of the oxide coverage among the Pt/C and Pt/Pd/C at 1.1 V (*vs* RHE). This clearly illustrates that the coverage in the Pt/Pd/C is affected by temperature more than that in the Pt/C and that the adsorption of oxide species is enhanced by higher temperatures in Pt/Pd/C. At 60 °C, the least oxide coverage was Pt/Pd(2.3)/C, whereas that of Pt/Pd(8.0)/C was dramatically increased, showing the same value as those in Pt/C. These trends agreed with the behavior of the apparent rate constants in Figure 2. Therefore, it can be suggested that the increase of the oxide coverage caused the significant activity decrease of Pt/Pd/C.

***Operando* XAS measurements.** In order to observe the temperature dependence of the oxide coverage on Pt, *operando* measurements were conducted. *Operando* Pt L_{III}-edge X-ray absorption near-edge structures (XANES) in Figures S16−S19 show the oxidation states of Pt atoms in the Pt/C and Pt/Pd/C. The XANES white line area change (ΔXANES) compared at 0.5 V for Pt/C and Pt/Pd/C catalyst at 25 and 60 °C is shown in Figure S20. ΔXANES was calculated from the following equation:

$$\Delta\text{XANES} = \text{area of white line at } (0.5 - 1.1\ \text{V vs RHE}) - \text{area of white line at } 0.5\ \text{V (V vs RHE)} \quad (1)$$

Here, the white line peak area increased with increasing temperature, revealing that the Pt shell on Pt/Pd/C shows much more adsorption of oxide species at 60 °C than at 25 °C. This agrees with the oxide coverage measurements shown in

https://dx.doi.org/10.1021/acsaem.0c02708
ACS Appl. Energy Mater. XXXX, XXX, XXX−XXX

Figure 3, indicating that the oxide species on the Pt shell could easily be influenced by temperature.

To understand the local structures, we fabricated a Pt layer model on the Pd according to our previous report[41] and calculated the phase shifts and the backscattering factors with the FEFF code. The fitted parameters are also shown in Tables S3−S6.

As mentioned above, the Pt−Pt bond length dependence has been reported as an important factor which could reflect the d-band center status and could be related to the ORR activity.[26,29] Figure 4a,b shows the fitting results for the Pt−Pt

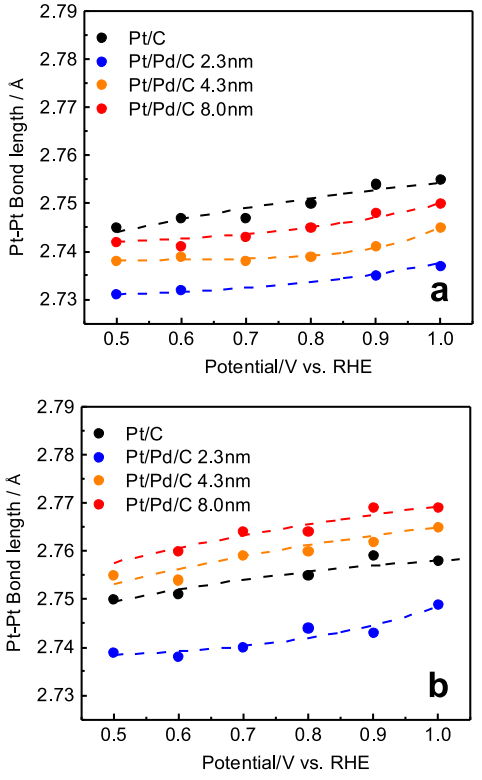

Figure 4. EXAFS fitting results for Pt−Pt bond distance of the nearest neighbors in Pt/C catalyst (black) and Pt/Pd/C catalyst synthesized on 2.3 nm (blue), 4.3 nm (orange), and 8.0 nm (red) diameter Pd core fitted from the corresponding EXAFS at 25 °C (a) and 60 °C (b).

bond distance of the Pt shell on each Pt/Pd/C at 25 and 60 °C in the range of 0.5 to 1.0 V *vs* RHE, whereas the Fourier transforms of EXAFS are shown in Figures S21−S24. The coordination numbers of Pt−Pt and Pd−Pd about the Pt/Pd/C and Pt/C catalysts are shown in Tables S3−S6. The coordination numbers of Pt−Pt and Pd−Pd on Pt/Pd/C and Pt/C catalysts are shown in Tables S2−S5. Pt−Pt coordination numbers were almost the same regardless of the temperature at 0.5 V in both Pt/Pd/C and Pt/C catalysts. The lower Pt−Pt coordination numbers were observed at higher potential and temperature due to Pt−O bond formation.

In terms of bond distance, Pt/C showed a Pt−Pt bond of 2.743 (±0.002 Å) at 0.5 V (*vs* RHE), which is slightly shorter than that of Pt foil (2.757 Å) at 25 °C. At 60 °C, the Pt−Pt distance of the Pt/C was slightly extended to 2.749 (±0.003 Å). In the case of the Pt/Pd/C at 25 °C, Pt/Pd(2.3)/C had a contraction of the Pt−Pt bond distance of 2.731 Å at 0.5 V (*vs* RHE), which was shorter than that of Pt/Pd(4.3)/C and Pt/Pd(8.0)/C. As the lattice shrinkage of Pd nanoparticles was observed with decreasing particle size owing to the nanosize effect,[56] the lattice strain effect of Pt atoms on the surface varies depending on the core size. As suggested by Kaito *et al.*,[57] the appropriate Pt−Pt bond shrinkage is expected to change the status of the d-band center and enhance the ORR activity. Therefore, the appropriate Pt−Pt bond distance on Pt/Pd(8.0)/C led to the best ORR activity for the Pt/Pd/C at 25 °C. In the case of Pt/Pd/C at 60 °C (Figure 4b), the Pt−Pt bond distance of Pt/Pd/C was extended compared to that at 25 °C. At 60 °C, Pt/Pd(2.3)/C still had the shortest Pt−Pt bond distance compared to the others. It can be expected that the activity of Pt/Pd(2.3)/C at 60 °C was improved thanks to the extension of the bond, which had shrunk too much at 25 °C. On the other hand, Pt/Pd(4.3)/C and Pt/Pd(8.0)/C suffered over an extended Pt−Pt bond because of the high-temperature environment at 60 °C. Therefore, we can conclude that the overextended Pt−Pt bond leads to dramatic oxide adsorption at the active sites on the Pt surface, which is the main reason for the decrease of k_{app} in the Pt/Pd/C at 60 °C. Moreover, we expect that the overextension of Pt−Pt bond distance at high temperatures on the Pd core surface should be the reason for the Pd atoms possessing a thermal expansion coefficient higher than that of Pt atoms.[58] The larger thermal expansion of Pd cores in Pt/Pd/C compared to that in Pt/C leads to the larger Pt−Pt bond extension of the Pt shell on the surface and causes a decrease in the ORR activity at 60 °C.

High-Temperature X-ray Diffraction. The Pt−Pt bond length extension on the Pd surface is expected to be caused by the larger thermal expansion coefficient of Pd with respect to Pt. The extra thermal expansion of nanosized materials also might be expected to contribute to the Pd core expansion. The *in situ* high-temperature X-ray diffraction results in Figure 5

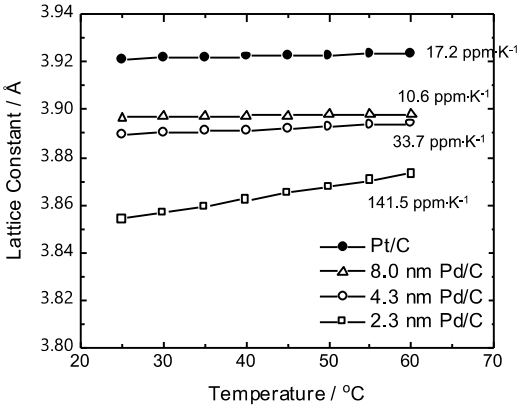

Figure 5. Lattice constant of Pt in Pt/C and 2.3, 4.3, and 8.0 nm diameter Pd nanoparticles in Pd/C from 25 to 80 °C, analyzed through *in situ* HT-XRD. The slope of the line in the figure indicates thermal expansion coefficient for each material.

and Figure S25 confirmed a difference in thermal expansion of the Pt/C and various particle-sized Pd/C. The Pd/C (141.5, 33.7 ppm·K^{-1}) and Pt/C (17.2 ppm·K^{-1}) possess a thermal expansion coefficient larger than that of bulk Pd and Pt, respectively, as established by another group.[59] The larger thermal expansion coefficient of Pd/C relative to Pt/C indicates that Pd core expansion will impose an additional thermal expansion on the Pt shell in the Pt/Pd/C. Therefore, we assumed that this Pt−Pt bond length extension in the Pt/Pd/C at high temperature is caused by the difference in the

https://dx.doi.org/10.1021/acsaem.0c02708
ACS Appl. Energy Mater. XXXX, XXX, XXX−XXX

thermal expansion coefficients between Pt and Pd as well as by the particle size effect.

In summary, the compressive strain on Pt/Pd(8.0)/C at 25 °C leads to the shorter Pt−Pt bond distance compared to that in the Pt/C catalyst, changes the position of d-band center, and improves the ORR activity. However, Pt/Pd(2.3)/C suffered over a compressive strain effect and led to a slight decrease of ORR activity. At 60 °C, due to the more significant thermal expansion of the Pd core in Pt/Pd/C than in Pt/C, the Pt shell in Pt/Pd/C exhibited a Pt−Pt bond length extension higher than that for Pt/C. The over expansion of the Pt−Pt bond length in the Pt shell on the Pt/Pd/C weakens the compressive strain effect, which causes a decrease in the ORR activity, as evidenced by *operando* XAS and *in situ* high-temperature X-ray diffraction.

CONCLUSION

This study investigated the effect of temperature on the ORR activity of a Pt shell−Pd core catalyst. The apparent rate constants (k_{app}), the coverage of oxide species, and the local structures were determined using electrochemical measurements and *operando* XAS. The apparent rate constant (k_{app}) in the Pt/Pd/C corresponded to an ORR activity higher than that of Pt/C at 25 °C, but the ORR activity started to decrease at high temperature (50−60 °C). Pt/Pd/C with a smaller core possess ORR activity lower than that of the a larger Pd core at 25 °C, but the ORR activity started to decrease at 60 °C. The coverage of Pt/Pd/C was much lower than that of Pt/C at 25 °C. However, it increased dramatically with the increasing temperature, and Pt/Pd/C with a larger Pd core got more of an oxygen coverage increase from 25 to 60 °C, which could be a partial reason for the decrease in the ORR activity. The *operando* XAS study showed that the Pt−Pt bond length of the Pt/Pd/C catalysts was shorter than that of the Pt/C due to the compressive surface strain on the Pd core. According to *operando* XAS and high-temperature X-ray diffraction, the Pt−Pt bond length extension was more significant for Pt/Pd/C catalysts than for Pt/C at 60 °C. The most significant Pt−Pt bond distance extension occurred on Pt/Pd/C with a larger Pd core, which could be the reason for a decrease in the ORR activity. This structural change of the catalyst was determined by the different thermal expansion between Pd core material and the Pt shell.

ASSOCIATED CONTENT

Supporting Information

The Supporting Information is available free of charge at https://pubs.acs.org/doi/10.1021/acsaem.0c02708.

Additional details of the UPD synthesis of Pt/Pd/C core−shell catalyst, CV and linear sweep voltammetry experiment of Pt/Pd/C and Pt/C at various temperatures (25−60 °C), *operando* XAS measurement details, and XAS data (PDF)

AUTHOR INFORMATION

Corresponding Author

Tomoki Uchiyama − *Graduate School of Human and Environmental Studies, Kyoto University, Kyoto 606-8501, Japan;* orcid.org/0000-0003-4880-7498; Email: uchiyama.tomoki.3x@kyoto-u.ac.jp

Authors

Chen Liu − *Graduate School of Human and Environmental Studies and Graduate School of Advanced Integrated Studies in Human Survivability (Shishu-Kan), Kyoto University, Kyoto 606-8501, Japan*

Kentaro Yamamoto − *Graduate School of Human and Environmental Studies, Kyoto University, Kyoto 606-8501, Japan;* orcid.org/0000-0002-8739-4246

Toshiki Watanabe − *Graduate School of Human and Environmental Studies, Kyoto University, Kyoto 606-8501, Japan*

Xiao Gao − *Graduate School of Human and Environmental Studies, Kyoto University, Kyoto 606-8501, Japan;* orcid.org/0000-0002-5469-1754

Hideto Imai − *Device Analysis Department, Nissan ARC, Ltd., Yokosuka, Kanagawa 237-0061, Japan;* orcid.org/0000-0002-9434-1492

Masashi Matsumoto − *Device Analysis Department, Nissan ARC, Ltd., Yokosuka, Kanagawa 237-0061, Japan*

Seiho Sugawara − *Fuel Cell Cutting-Edge Research Center Technology Research Association (FC-Cubic), Tokyo 135-0064, Japan*

Kazuhiko Shinohara − *Fuel Cell Cutting-Edge Research Center Technology Research Association (FC-Cubic), Tokyo 135-0064, Japan*

Koichiro Oshima − *Graduate School of Advanced Integrated Studies in Human Survivability (Shishu-Kan), Kyoto University, Kyoto 606-8306, Japan*

Shigeki Sakurai − *Graduate School of Advanced Integrated Studies in Human Survivability (Shishu-Kan), Kyoto University, Kyoto 606-8306, Japan*

Yoshiharu Uchimoto − *Graduate School of Human and Environmental Studies, Kyoto University, Kyoto 606-8501, Japan;* orcid.org/0000-0002-1491-2647

Complete contact information is available at: https://pubs.acs.org/10.1021/acsaem.0c02708

Funding

This work is based on results obtained from a project (JPNP15001, JPNP20003) commissioned by the New Energy and Industrial Technology Development Organization (NEDO) of Japan.

Notes

The authors declare no competing financial interest.

ACKNOWLEDGMENTS

The authors thank for Dr. Hidekazu Sugimori, Dr. Takeshi Terao, and Dr. Toshie Furuya at FC-cubic and Nissan ARC for providing TEM images. The synchrotron radiation experiments were performed at the BL37XU, BL01B1, BL02B2, and BL19B2 beamline of SPring-8 with the approval of the Japan Synchrotron Radiation Research Institute (JASRI) (Proposal Nos. 2016B1517, 2017A1456, 2017B1043, 2017B1055, and 2018A1019). This work was supported by the Polymer Membrane Fuel Cell Project (JPNP15001, JPNP20003) of the New Energy and Industrial Technology Development Organization (NEDO) of Japan.

REFERENCES

(1) Hamada, Y.; Goto, R.; Nakamura, M.; Kubota, H.; Ochifuji, K. Operating results and simulations on a fuel cell for residential energy systems. *Energy Convers. Manage.* **2006**, *47* (20), 3562−3571.

(2) Hamada, Y.; Nakamura, M.; Kubota, H.; Ochifuji, K.; Murase, M.; Goto, R. Field performance of a polymer electrolyte fuel cell for a residential energy system. *Renewable Sustainable Energy Rev.* **2005**, *9* (4), 345−362.
(3) Hamada, Y.; Takeda, K.; Goto, R.; Kubota, H. Hybrid utilization of renewable energy and fuel cells for residential energy systems. *Energy and Buildings* **2011**, *43* (12), 3680−3684.
(4) Bocci, E.; Zuccari, F.; Dell'Era, A. Renewable and hydrogen energy integrated house. *Int. J. Hydrogen Energy* **2011**, *36* (13), 7963−7968.
(5) Staffell, I.; Scamman, D.; Velazquez Abad, A.; Balcombe, P.; Dodds, P. E.; Ekins, P.; Shah, N.; Ward, K. R. The role of hydrogen and fuel cells in the global energy system. *Energy Environ. Sci.* **2019**, *12* (2), 463−491.
(6) Aoki, N.; Inoue, H.; Shirai, A.; Higuchi, S.; Matsui, Y.; Daimon, H.; Doi, T.; Inaba, M. Electrochemical and Chemical Treatment Methods for Enhancement of Oxygen Reduction Reaction Activity of Pt Shell-Pd Core Structured Catalyst. *Electrochim. Acta* **2017**, *244*, 146−153.
(7) Takenaka, S.; Goto, M.; Masuda, Y.; Emura, S.; Kishida, M. Improvement in the durability of carbon black-supported Pt cathode catalysts by silica-coating for use in PEFCs. *Int. J. Hydrogen Energy* **2018**, *43* (15), 7473−7482.
(8) Sundmacher, K. Fuel Cell Engineering: Toward the Design of Efficient Electrochemical Power Plants. *Ind. Eng. Chem. Res.* **2010**, *49* (21), 10159−10182.
(9) Rabis, A.; Rodriguez, P.; Schmidt, T. J. Electrocatalysis for Polymer Electrolyte Fuel Cells: Recent Achievements and Future Challenges. *ACS Catal.* **2012**, *2* (5), 864−890.
(10) Song, L.; Liang, Z.; Nagamori, K.; Igarashi, H.; Vukmirovic, M. B.; Adzic, R. R.; Sasaki, K. Enhancing Oxygen Reduction Performance of Pt Monolayer Catalysts by Pd(111) Nanosheets on WNi Substrates. *ACS Catal.* **2020**, *10*, 4290−4298.
(11) Song, L.; Liang, Z.; Vukmirovic, M. B.; Adzic, R. R. Enhanced Oxygen Reduction Reaction Activity on Pt-Monolayer-Shell PdIr/Ni-Core Catalysts. *J. Electrochem. Soc.* **2018**, *165*, J3288−J3294.
(12) Nilekar, A. U.; Xu, Y.; Zhang, J. L.; Vukmirovic, M. B.; Sasaki, K.; Adzic, R. R.; Mavrikakis, M. Bimetallic and ternary alloys for improved oxygen reduction catalysis. *Top. Catal.* **2007**, *46* (3−4), 276−284.
(13) Wang, J. X.; Inada, H.; Wu, L. J.; Zhu, Y. M.; Choi, Y. M.; Liu, P.; Zhou, W. P.; Adzic, R. R. Oxygen Reduction on Well-Defined Core-Shell Nanocatalysts: Particle Size, Facet, and Pt Shell Thickness Effects. *J. Am. Chem. Soc.* **2009**, *131* (47), 17298−17302.
(14) Sasaki, K.; Wang, J. X.; Naohara, H.; Marinkovic, N.; More, K.; Inada, H.; Adzic, R. R. Recent advances in platinum monolayer electrocatalysts for oxygen reduction reaction: Scale-up synthesis, structure and activity of Pt shells on Pd cores. *Electrochim. Acta* **2010**, *55* (8), 2645−2652.
(15) Sasaki, K.; Naohara, H.; Cai, Y.; Choi, Y. M.; Liu, P.; Vukmirovic, M. B.; Wang, J. X.; Adzic, R. R. Core-Protected Platinum Monolayer Shell High-Stability Electrocatalysts for Fuel-Cell Cathodes. *Angew. Chem., Int. Ed.* **2010**, *49* (46), 8602−8607.
(16) Sasaki, K.; Naohara, H.; Choi, Y. M.; Cai, Y.; Chen, W. F.; Liu, P.; Adzic, R. R. Highly stable Pt monolayer on PdAu nanoparticle electrocatalysts for the oxygen reduction reaction. *Nat. Commun.* **2012**, *3*, 1115.
(17) Chen, C.; Kuttiyiel, K. A.; Li, M.; Su, D.; Du, L.; Du, C.; Gao, Y.; Fei, W.; Yin, G.; Sasaki, K.; Adzic, R. R. Correlating the electrocatalytic stability of platinum monolayer catalysts with their structural evolution in the oxygen reduction reaction. *J. Mater. Chem. A* **2018**, *6*, 20725−20736.
(18) Inaba, M.; Daimon, H. Development of Highly Active and Durable Platinum Core-shell Catalysts for Polymer Electrolyte Fuel Cells. *J. Jpn. Pet. Inst.* **2015**, *58* (2), 55−63.
(19) Liu, W.; Rodriguez, P.; Borchardt, L.; Foelske, A.; Yuan, J. P.; Herrmann, A. K.; Geiger, D.; Zheng, Z. K.; Kaskel, S.; Gaponik, N.; Kotz, R.; Schmidt, T. J.; Eychmuller, A. Bimetallic Aerogels: High-Performance Electrocatalysts for the Oxygen Reduction Reaction. *Angew. Chem., Int. Ed.* **2013**, *52* (37), 9849−9852.
(20) Oezaslan, M.; Herrmann, A.-K.; Werheid, M.; Frenkel, A. I.; Nachtegaal, M.; Dosche, C.; Laugier Bonnaud, C.; Yilmaz, H. C.; Kuhn, L.; Rhiel, E.; Gaponik, N.; Eychmuller, A.; Schmidt, T. J. Structural Analysis and Electrochemical Properties of Bimetallic Palladium-Platinum Aerogels Prepared by a Two-Step Gelation Process. *ChemCatChem* **2017**, *9* (5), 798−808.
(21) Oezaslan, M.; Liu, W.; Nachtegaal, M.; Frenkel, A. I.; Rutkowski, B.; Werheid, M.; Herrmann, A. K.; Laugier-Bonnaud, C.; Yilmaz, H. C.; Gaponik, N.; Czyrska-Filemonowicz, A.; Eychmuller, A.; Schmidt, T. J. Homogeneity and elemental distribution in self-assembled bimetallic Pd-Pt aerogels prepared by a spontaneous one-step gelation process. *Phys. Chem. Chem. Phys.* **2016**, *18* (30), 20640−20650.
(22) Wongkaew, A.; Zhang, Y.; Tengco, J. M. M.; Blom, D. A.; Sivasubramanian, P.; Fanson, P. T.; Regalbuto, J. R.; Monnier, J. R. Characterization and Evaluation of Pt-Pd Electrocatalysts Prepared by Electroless Deposition. *Appl. Catal., B* **2016**, *188*, 367−375.
(23) You, D. J.; Kim, D. H.; De Lile, J. R.; Li, C.; Lee, S. G.; Kim, J. M.; Pak, C. Pd core-shell alloy catalysts for high-temperature polymer electrolyte membrane fuel cells: Effect of the core composition on the activity towards oxygen reduction reactions. *Appl. Catal., A* **2018**, *562*, 250−257.
(24) Yun, S.; Ted Oyama, S. Correlations in palladium membranes for hydrogen separation: A review. *J. Membr. Sci.* **2011**, *375* (1−2), 28−45.
(25) Gao, H.; Liao, S.; Zhang, Y.; Wang, L.; Zhang, L. Methanol tolerant core-shell RuFeSe@Pt/C catalyst for oxygen reduction reaction. *Int. J. Hydrogen Energy* **2017**, *42* (32), 20658−20668.
(26) Shao, M. H.; Shoemaker, K.; Peles, A.; Kaneko, K.; Protsailo, L. Pt Mono layer on Porous Pd-Cu Alloys as Oxygen Reduction Electrocatalysts. *J. Am. Chem. Soc.* **2010**, *132* (27), 9253−9255.
(27) Kong, F.; Ren, Z.; Norouzi Banis, M.; Du, L.; Zhou, X.; Chen, G.; Zhang, L.; Li, J.; Wang, S.; Li, M.; Doyle-Davis, K.; Ma, Y.; Li, R.; Young, A.; Yang, L.; Markiewicz, M.; Tong, Y.; Yin, G.; Du, C.; Luo, J.; Sun, X. Active and Stable Pt−Ni Alloy Octahedra Catalyst for Oxygen Reduction via Near-Surface Atomical Engineering. *ACS Catal.* **2020**, *10*, 4205−4214.
(28) Zhang, G.; Shao, Z. G.; Lu, W.; Xie, F.; Xiao, H.; Qin, X.; Yi, B. Core−shell Pt modified Pd/C as an active and durable electrocatalyst for the oxygen reduction reaction in PEMFCs. *Appl. Catal., B* **2013**, *132−133*, 183−194.
(29) Wang, X.; Orikasa, Y.; Inaba, M.; Uchimoto, Y. Reviving Galvanic Cells To Synthesize Core-Shell Nanoparticles with a Quasi-Monolayer Pt Shell for Electrocatalytic Oxygen Reduction. *ACS Catal.* **2020**, *10* (1), 430−434.
(30) Rück, M.; Garlyyev, B.; Mayr, F.; Bandarenka, A. S.; Gagliardi, A. Oxygen Reduction Activities of Strained Platinum Core-Shell Electrocatalysts Predicted by Machine Learning. *J. Phys. Chem. Lett.* **2020**, *11* (5), 1773−1780.
(31) Kongkanand, A.; Subramanian, N. P.; Yu, Y. C.; Liu, Z. Y.; Igarashi, H.; Muller, D. A. Achieving High-Power PEM Fuel Cell Performance with an Ultralow-Pt-Content Core-Shell Catalyst. *ACS Catal.* **2016**, *6* (3), 1578−1583.
(32) Gasteiger, H. A.; Kocha, S. S.; Sompalli, B.; Wagner, F. T. Activity benchmarks and requirements for Pt, Pt-alloy, and non-Pt oxygen reduction catalysts for PEMFCs. *Appl. Catal., B* **2005**, *56* (1−2), 9−35.
(33) Gasteiger, H. A.; Panels, J. E.; Yan, S. G. Dependence of PEM fuel cell performance on catalyst loading. *J. Power Sources* **2004**, *127* (1−2), 162−171.
(34) Pedersen, C. M.; Escudero-Escribano, M.; Velazquez-Palenzuela, A.; Christensen, L. H.; Chorkendorff, I.; Stephens, I. E. L. Benchmarking Pt-based electrocatalysts for low temperature fuel cell reactions with the rotating disk electrode: oxygen reduction and hydrogen oxidation in the presence of CO (review article). *Electrochim. Acta* **2015**, *179*, 647−657.

https://dx.doi.org/10.1021/acsaem.0c02708
ACS Appl. Energy Mater. XXXX, XXX, XXX−XXX

(35) Rajalakshmi, N.; Raja, M.; Dhathathreyan, K. S. Evaluation of current distribution in a proton exchange membrane fuel cell by segmented cell approach. *J. Power Sources* **2002**, *112* (1), 331−336.
(36) Noponen, M.; Hottinen, T.; Mennola, T.; Mikkola, M.; Lund, P. Determination of mass diffusion overpotential distribution with flow pulse method from current distribution measurements in a PEMFC. *J. Appl. Electrochem.* **2002**, *32* (10), 1081−1089.
(37) Kongkanand, A.; Ziegelbauer, J. M. Surface Platinum Electrooxidation in the Presence of Oxygen. *J. Phys. Chem. C* **2012**, *116* (5), 3684−3693.
(38) Wakabayashi, N.; Takeichi, M.; Itagaki, M.; Uchida, H.; Watanabe, M. Temperature-dependence of oxygen reduction activity at a platinum electrode in an acidic electrolyte solution investigated with a channel flow double electrode. *J. Electroanal. Chem.* **2005**, *574* (2), 339−346.
(39) Yano, H.; Akiyama, T.; Uchida, H.; Watanabe, M. Temperature dependence of oxygen reduction activity at Nafion-coated Pt/graphitized carbon black catalysts prepared by the nanocapsule method. *Energy Environ. Sci.* **2010**, *3* (10), 1511−1514.
(40) Wang, X.; Orikasa, Y.; Uchimoto, Y. Platinum-Based Electrocatalysts for the Oxygen-Reduction Reaction: Determining the Role of Pure Electronic Charge Transfer in Electrocatalysis. *ACS Catal.* **2016**, *6* (7), 4195−4198.
(41) Wang, X.; Orikasa, Y.; Takesue, Y.; Inoue, H.; Nakamura, M.; Minato, T.; Hoshi, N.; Uchimoto, Y. Quantitating the Lattice Strain Dependence of Monolayer Pt Shell Activity toward Oxygen Reduction. *J. Am. Chem. Soc.* **2013**, *135* (16), 5938−5941.
(42) Zhang, J.; Lima, F. H. B.; Shao, M. H.; Sasaki, K.; Wang, J. X.; Hanson, J.; Adzic, R. R. Platinum monolayer on nonnoble metal-noble metal core-shell nanoparticle electrocatalysts for O_2 reduction. *J. Phys. Chem. B* **2005**, *109* (48), 22701−22704.
(43) Vukmirovic, M. B.; Zhang, J.; Sasaki, K.; Nilekar, A. U.; Uribe, F.; Mavrikakis, M.; Adzic, R. R. Platinum monolayer electrocatalysts for oxygen reduction. *Electrochim. Acta* **2007**, *52* (6), 2257−2263.
(44) Russell, A. E.; Rose, A. X-ray absorption Spectroscopy of low temperature fuel cell catalysts. *Chem. Rev.* **2004**, *104* (10), 4613−4635.
(45) Kong, F.; Liu, S.; Li, J.; Du, L.; Banis, M. N.; Zhang, L.; Chen, G.; Doyle-Davis, K.; Liang, J.; Wang, S.; Zhao, F.; Li, R.; Du, C.; Yin, G.; Zhao, Z.; Sun, X. Trimetallic Pt−Pd−Ni octahedral nanocages with subnanometer thick-wall towards high oxygen reduction reaction. *Nano Energy* **2019**, *64*, 103890.
(46) Sasaki, K.; Marinkovic, N.; Isaacs, H. S.; Adzic, R. R. Synchrotron-Based In Situ Characterization of Carbon-Supported Platinum and Platinum Monolayer Electrocatalysts. *ACS Catal.* **2016**, *6*, 69−76.
(47) Nagasawa, K.; Takao, S.; Nagamatsu, S.; Samjeske, G.; Sekizawa, O.; Kaneko, T.; Higashi, K.; Yamamoto, T.; Uruga, T.; Iwasawa, Y. Surface-Regulated Nano-SnO_2/Pt_3Co/C Cathode Catalysts for Polymer Electrolyte Fuel Cells Fabricated by a Selective Electrochemical Sn Deposition Method. *J. Am. Chem. Soc.* **2015**, *137* (40), 12856−12864.
(48) Zhao, X.; Takao, S.; Higashi, K.; Kaneko, T.; Samjeske, G.; Sekizawa, O.; Sakata, T.; Yoshida, Y.; Uruga, T.; Iwasawa, Y. Simultaneous Improvements in Performance and Durability of an Octahedral PtNix/C Electrocatalyst for Next-Generation Fuel Cells by Continuous, Compressive, and Concave Pt Skin Layers. *ACS Catal.* **2017**, *7* (7), 4642−4654.
(49) Kumar, A.; Buttry, D. A. Size-Dependent Underpotential Deposition of Copper on Palladium Nanoparticles. *J. Phys. Chem. C* **2015**, *119* (29), 16927−16933.
(50) Liu, Y. X.; Mathias, M.; Zhang, J. L. Measurement of Platinum Oxide Coverage in a Proton Exchange Membrane Fuel Cell. *Electrochem. Solid-State Lett.* **2010**, *13* (1), B1−B3.
(51) Imai, H.; Izumi, K.; Matsumoto, M.; Kubo, Y.; Kato, K.; Imai, Y. In Situ and Real-Time Monitoring of Oxide Growth in a Few Monolayers at Surfaces of Platinum Nanoparticles in Aqueous Media. *J. Am. Chem. Soc.* **2009**, *131* (17), 6293−6300.
(52) Dang, D.; Zou, H.; Xiong, Z.; Hou, S.; Shu, T.; Nan, H.; Zeng, X.; Zeng, J.; Liao, S. High-Performance, Ultralow Platinum Membrane Electrode Assembly Fabricated by In Situ Deposition of a Pt Shell Layer on Carbon-Supported Pd Nanoparticles in the Catalyst Layer Using a Facile Pulse Electrodeposition Approach. *ACS Catal.* **2015**, *5* (7), 4318−4324.
(53) Gomez, R.; Orts, J. M.; Alvarez-Ruiz, B.; Feliu, J. M. Effect of temperature on hydrogen adsorption on Pt(111), Pt(110), and Pt(100) electrodes in 0.1 M $HClO_4$. *J. Phys. Chem. B* **2004**, *108* (1), 228−238.
(54) He, D.; He, D.; Wang, J.; Lin, Y.; Yin, P.; Hong, X.; Wu, Y.; Li, Y. Ultrathin Icosahedral Pt-Enriched Nanocage with Excellent Oxygen Reduction Reaction Activity. *J. Am. Chem. Soc.* **2016**, *138* (5), 1494−1497.
(55) Liu, Y.; Liu, S.; Che, Z.; Zhao, S.; Sheng, X.; Han, M.; Bao, J. Concave octahedral Pd@PdPt electrocatalysts integrating core−shell, alloy and concave structures for high-efficiency oxygen reduction and hydrogen evolution reactions. *J. Mater. Chem. A* **2016**, *4*, 16690−16697.
(56) Lamber, R.; Wetjen, S.; Jaeger, N. I. Size dependence of the lattice parameter of small palladium particles. *Phys. Rev. B: Condens. Matter Mater. Phys.* **1995**, *51*, 10968−1097.
(57) Kaito, T.; Tanaka, H.; Mitsumoto, H.; Sugawara, S.; Shinohara, K.; Ariga, H.; Uehara, H.; Takakusagi, S.; Asakura, K. *In Situ* X-ray Absorption Fine Structure Analysis of PtCo, PtCu, and PtNi Alloy Electrocatalysts: The Correlation of Enhanced Oxygen Reduction Reaction Activity and Structure. *J. Phys. Chem. C* **2016**, *120* (21), 11519−11527.
(58) Fred, R. *Handbook of Electron Tube and Vacuum Techniques*; American Institute of Physics: New York, 1993; p 26.
(59) Leontyev, I. N.; Kulbakov, A. A.; Allix, M.; Rakhmatullin, A.; Kuriganova, A. B.; Maslova, O. A.; Smirnova, N. V. Thermal expansion coefficient of carbon-supported Pt nanoparticles: In-situ X-ray diffraction study. *Phys. Status Solidi B* **2017**, *254* (5), 1600695.

https://dx.doi.org/10.1021/acsaem.0c02708
ACS Appl. Energy Mater. XXXX, XXX, XXX−XXX